# Strain tunable interlayer and intralayer excitons in vertically stacked $MoSe_2/WSe_2$ heterobilayers

# Strain tunable interlayer and intralayer excitons in vertically stacked $MoSe_2/WSe_2$ heterobilayers

L. L. Li,[1,2,*] R. Gillen,[3,†] M. Palummo,[4,‡] M. V. Milošević,[2,§] and F. M. Peeters[2,¶]

[1]*School of Physics and Optoelectronic Engineering, Nanjing University of Information Science and Technology, Nanjing 210044, China*
[2]*Department of Physics, University of Antwerp, Groenenborgerlaan 171, 2020 Antwerpen, Belgium*
[3]*Friedrich-Alexander Universität Erlangen-Nürnberg, Staudtstrasse 7, 91058 Erlangen, Germany*
[4]*Dipartimento di Fisica and INFN, Universitá di Roma "Tor Vergata", Via della Ricerca Scientifica 1, 00133 Rome, Italy*

(Dated: August 31, 2023)

Recently interlayer and intralayer excitons in transition metal dichalcogenide (TMD) heterobilayers have been studied both experimentally and theoretically. In spite of a growing interest, these layer-resolved excitons in the presence of external stimuli such as strain remain not fully understood. Here, using density-functional theory calculations with many-body effects, we explore the excitonic properties of vertically stacked $MoSe_2/WSe_2$ heterobilayer in the presence of in-plane biaxial strain of up to 5%. We calculate the strain dependence of exciton absorption spectrum, oscillator strength, wave function, and binding energy by solving the Bethe-Salpeter equation on top of the standard GW approach. We identify the interlayer and intralayer excitons by analysing their electron-hole weights and spatial wave functions. We show that with increasing strain magnitude, the absorption spectrum of the interlayer and intralayer excitons is red-shifted and re-ordered, and the binding energies of these layer-resolved excitons decrease monotonically and almost linearly. We derive the sensitivity of exciton binding energy to the applied strain and find that the intralayer excitons are more sensitive to strain than the interlayer excitons. For instance, a sensitivity of $-7.9$ meV/% is derived for the intra-$MoSe_2$-layer excitons, which is followed by $-7.4$ meV/% for the intra-$WSe_2$-layer excitons, and by$-4.2$ meV/% for the interlayer excitons. Our results indicate that interlayer and intralayer excitons in vertically stacked $MoSe_2/WSe_2$ heterobilayer are efficiently tunable by in-plane biaxial strain.

Monolayer transition metal dichalcogenides (TMDs) with the structural formula $MX_2$ ($M$ = Mo/W and $X$ = S/Se/Te) exhibit high carrier mobility and strong light-matter interaction, which makes them very promising for atomically thin electronics and optoelectronics[1–4]. Due to their atomically thin character, strong quantum confinement and weak dielectric screening give rise to significantly enhanced Coulomb interaction. This leads to the formation of tightly bound excitons with typical binding energies of 0.3-0.7 eV[5–10], which dominate the optical properties of monolayer TMDs at both cryogenic and room temperatures[11]. Moreover, monolayer TMDs exhibit a rich excitonic spectrum featured by $A$ and $B$ excitons in lower-energy regime due to strong spin-orbit coupling of heavy TM atoms[12–16] and by $C$ excitons in higher-energy regime due to high joint density of states induced by band nesting in the Brillouin zone[17–19]. In parallel, other exciton complexes, such as charged excitons (trions) and biexcitons have also been investigated[20–25].

Different TMD monolayers can be combined to create vertical or lateral van der Waals (vdW) heterostructures, which can exhibit fascinating properties that are not present in their constituent monolayers, e.g., offering the possibility for the formation of both interlayer and intralayer excitons. Many-body effects due to interlayer excitons are expected to be of significant importance in TMD vdW heterostructures with type-II band alignment. For instance, in the independent-particle picture, the interlayer electronic transition is the lowest energy transition in optical absorption spectrum, while the spectral ordering of interlayer and intralayer excitons could possibly be reversed because the exciton binding energy is strongly enhanced in atomically thin systems. Recently, Mo- and W-based vertical vdW heterostructures have drawn a growing interest due to the observation of long-lived excitations (with typical lifetimes of 1-100 ns) in their optical spectra[26–31], which are absent in the optical spectra of their constituent monolayers. The origin of those long-lived excitations remains not entirely understood and depends on material combinations as well as experimental conditions. A reasonable and popular explanation is that due to the type-II band alignment of Mo- and W-based TMD layers[32], those long-lived excitations were attributed to *interlayer excitons* with a spatial separation of coupled electrons and holes residing in different TMD layers. In order to gain better understanding with more details, reliable and accurate theoretical calculations have been carried out and so far there have been a few theoretical studies based on density functional theory (DFT) and many-body perturbation theory (MBPT) exploring excitonic effects in Mo- and W-based heterobilayers[33–36]. These experimental and theoretical studies have shown that interlayer excitons are of lower excitation energy, far smaller oscillator strength, and comparable binding energy compared to intralayer excitons. It has also been shown both experimentally and theoretically that interlayer excitons of finite momentum (i.e. momentum-indirect interlayer excitons) are important for the understanding of the main charactersitic peaks in the optical spectra of TMD systems[37–41] . Moreover, twist-dependent moiré excitons have also been investigated in TMD systems both experimentally and theoretically[42–52].

TMD monolayers are known to exhibit superior mechanical strength due to their atomically thin nature, e.g., monolayer $MoS_2$ can withstand a large-magnitude strain of up to 10% before its rupture[53]. Strain engineering has been demonstrated as an efficient approach to modulate the electronic and excitonic properties of atomically thin TMD systems[54–68], where for excitonic properties either (intralayer) excitons in TMD monolayers or interlayer excitons in TMD bilayers modulated by strain were investigated. In the present work, we perform systematic DFT and MBPT calculations to explore the ex-

citonic properties of vertically stacked $MoSe_2$/$WSe_2$ heterobilayer in the presence of in-plane biaxial strain. By solving the Bethe-Salpeter equation (BSE) on top of the standard GW approach, we calculate the strain dependence of both interlayer and intralayer excitons in terms of their absorption spectra, oscillator strengths, wave functions, and binding energies. Here, we identify interlayer and intralayer excitons by analysing their electron-hole weights (in reciprocal space) and wave functions (in real space). We show that their absorption spectra, oscillator strengths, wave functions, and binding energies can efficiently be tuned by the applied strain.

Fig. 1(a) shows the optimized lattice structure of unstrained vertical $MoSe_2$/$WSe_2$ heterobilayer with $AA'$ stacking (a 180-degree relative rotation between the two monolayers), where the chalcogen atoms in one monolayer are aligned with the metal atoms in the other monolayer. The in-plane lattice constant and the interlayer distance of this $AA'$-stacked heterobilayer obtained from our calculations are 3.29 Å and 6.52 Å, respectively, which are in agreement with previous theoretical work[34]. Typically there are three different stackings (i.e., $AA$, $AA'$, and $AB$) in vertically stacked TMD heterobilayers, where $AA$ corresponds to no relative shift and rotation between the two monolayers while $AB$ corresponds to no relative rotation but a relative shift between the two monolayers such that the chalcogen atoms in one monolayer are aligned with the centers of the metal-chalcogen hexagons in the other monolayer. Our calculations indicate that the different stackings have a negligible effect on the in-plane lattice constants and that the $AA'$ stacking is energetically the most stable as compared to the $AA$ and $AB$ stackings (see Table. S1 in Supplemental Material), which are also in agreement with previous theoretical work[34]. In what follows, we took the optimized lattice structure of vertically $AA'$-stacked $MoSe_2$/$WSe_2$ heterobilayer to calculate the quasi-particle and excitonic properties in the presence of in-plane biaxial tensile strain using the $G_0W_0$+BSE approach including electron-electron, electron-hole, and spin-orbit interactions.

Fig. 1(b) shows the DFT and $G_0W_0$ band structures of vertically $AA'$-stacked $MoSe_2$/$WSe_2$ heterobilayer in the absence of strain ($\epsilon = 0$). To facilitate our electronic analysis, we projected the band structures onto the $MoSe_2$ and $WSe_2$ layers, as indicated by red and blue, respectively. As seen, the valence band maximum (VBM) is of prevailing $WSe_2$ character while the conduction band minimum (CBM) is of dominant $MoSe_2$ character, leading to the so-called type-II band alignment[32]. Therefore, electrons and holes are mainly localized in the $MoSe_2$ and $WSe_2$ layers, respectively, i.e., they are spatially separated due to this type-II band alignment. This is the origin of the formation of interlayer excitons in vertically stacked $MoSe_2$/$WSe_2$ heterobilayer. Because the VBM (CBM) is located at the K (Q) point, the DFT and $G_0W_0$ band gaps are globally indirect, which are 0.99 eV and 1.74 eV, respectively. The direct band gaps for DFT and $G_0W_0$ are located at the K point, which are 1.11 eV and 1.97 eV, respectively, resulting in a quasi-particle correction of 0.86 eV to the single-particle energies. In the presence of strain ($\epsilon > 0$) and with increasing $\epsilon$ up to $5\%$, the direct band gaps for DFT and $G_0W_0$ decrease almost linearly whereas their indirect counterparts first increase then decrease, exhibiting a turning point at $\epsilon = 1\%$, as shown in Fig. 1(d). The DFT band gaps are globally direct for $\epsilon = 1\%$ and $2\%$ while indirect for $\epsilon = 0$, $3\%$, $4\%$, and $5\%$. However, due to the quasi-particle correction, the $G_0W_0$ band gaps are globally direct for $\epsilon = 2\%$ and $3\%$ while indirect for $\epsilon = 0$, $1\%$, $4\%$, and $5\%$. The competition between the globally direct and indirect band gaps for DFT and $G_0W_0$ can be understood with the location of the CBM and VBM in the corresponding band structures, as shown in Fig. 1(c). For instance, in the $G_0W_0$ band structures, the VBM and CBM are located at K and Q, respectively, for zero and $1\%$ strain, while the CBM is shifted from Q to K for $2\%$ and $3\%$ strain, leading to a direct band gap, and for $4\%$ and $5\%$ strain, the VBM is shifted as well, from K to $\Gamma$, restoring to an indirect band gap (see Fig. S6 in the Supplemental Material for more detail). If the convergence is further increased (e.g. the number of bands and the number of kpoints), the general feature of the $G_0W_0$ band gap should remain the same, i.e., it undergoes globally from indirect to direct and back to indirect. However, the critical strain values at those transitions are expected to be different than $2\%$ and $3\%$.

Fig. 2(a) shows the strain ($\epsilon$) dependence of the absorption spectrum and oscillator strength of the exciton states in vertically $AA'$-stacked $MoSe_2$/$WSe_2$ heterobilayer, which was obtained by solving the BSE on top of the $G_0W_0$ band structure. As can be seen, the absorption spectrum is clearly red-shifted (i.e. shifted to the lower excitation energy) with increasing $\epsilon$ from 0 to 5%. The on-set of absorption is dominated by the three excitonic states $X_1$, $X_2$, and $X_3$ as indicated. By analysing the electron-hole weights shown in Fig. 2(b) and the spatial wave functions shown in Fig. 2(c), we identify the interlayer exciton $X_1$ (electrons are localized in the $MoSe_2$ layer whereas holes are localized in $WSe_2$ layer) and the intralayer excitons $X_2$ (both electrons and holes are localized in the $MoSe_2$ layer) and $X_3$ (both electron and holes are localized in the $WSe_2$ layer). Here, the exciton wave functions shown in Fig. 2(c) were obtained in the absence of strain (their difference to those in the presence of strain is shown in Fig. S3 in the Supplemental Material). For all the considered strain, the interlayer exciton $X_1$ has lower excitation energy and much smaller oscillator strength than the intralyer excitons $X_2$ and $X_3$, as shown in the inset of Fig. 2(a). This is because interlayer excitons are formed by spatially separated electrons and holes residing in two different layers with type-II band alignment and thus their wave-function overlap is substantially reduced. However, the spectral ordering of the intralyer excitons $X_2$ and $X_3$ exhibits a cross-over behavior when the magnitude of strain increases from 0 to 5%: The excitation energy of $X_2$ is consistently smaller than that of $X_3$ for $0 <= \epsilon <= 2\%$, whereas the former is consistently larger than the latter for $3\% <= \epsilon <= 5\%$. This is convinced by looking into the strain dependence of the electron-hole weights of the $X_2$ and $X_3$ excitons, as shown in Fig. 2(b). By further inspecting the **k** dependence of those electron-hole weights, we find that both the interlayer and intralayer excitons are mainly localized around the K point in the quasi-particle band structure, i.e., the interlayer and intralayer K-excitons.

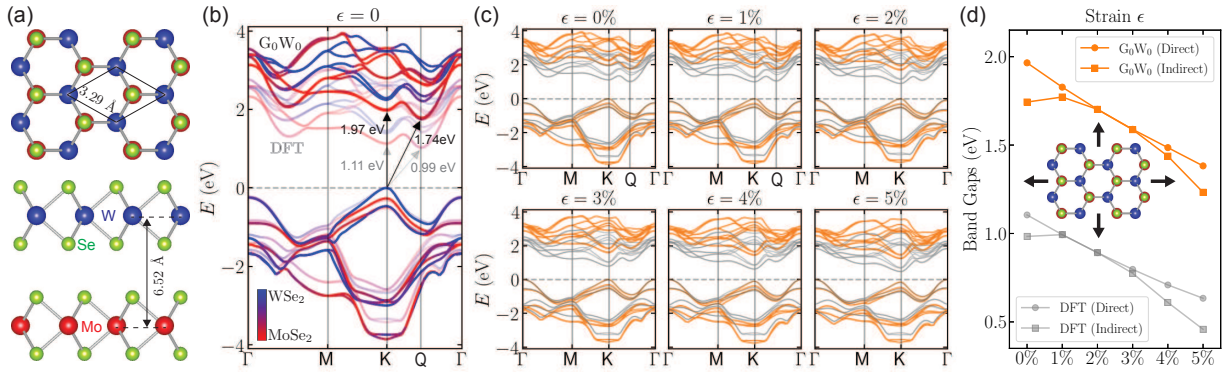


Figure 1. (a) The optimized lattice structure and (b) the DFT/$G_0W_0$ band structures of vertically $AA'$-stacked $MoSe_2$/$WSe_2$ heterobilayer in the absence of strain. (c) The DFT/$G_0W_0$ band structures and (d) the corresponding band gaps as a function of strain. Here, the color coding in (b) indicates the atomic projection of the band structure onto the $MoSe_2$ (red) and $WSe_2$ (blue) layers, the dashed lines in (b) and (c) represent the energetic position of the valence band maximum, and the black arrows in (d) denote the application of an in-plane biaxial tensile strain.

Regarding the optical absorption of excitons, it is of essential importance to relate our theoretical results to those experimental findings. One of the most recent experiments reported on the direct measurement of the optical absorption of interlayer excitons in $MoSe_2$/$WSe_2$ moire heterobilayers, which was accessed using their electric dipoles by effectively interpolating between $AA$ to $AB$ stackings[52]. Our calculations of the optical absorption of interlayer excitons in $AA'$-stacked MoSe2/WSe2 heterobilayer, when extended to be performed on a range of other stackings sampled along the stacking path from $AA$ to $AB$, may provide useful insights into some of the variations observed in experiments on $MoSe_2$/$WSe_2$ moire heterobilayers, particularly by well-defined local stackings in such moire systems.

It should be noted that the spectral ordering and the crossing behavior of the $X_2$ and $X_3$ excitons in the presence of strain, as shown in Fig. 2(a), could be affected by the way of how spin-orbit coupling (SOC) is included from DFT to GW and BSE calculations. We noticed that there are mainly two different approaches to including SOC in TMD systems in the literature. The first approach is to include SOC *partly* from DFT to GW+BSE calculations[69]: It calculates the DFT wave functions by turning off SOC at first, with which to calculate single-particle Green's function and screened Coulomb interaction; then SOC is turned on to perform the GW and BSE calculations by rediagonalizing the corresponding Hamiltonians. The second approach is to include SOC *fully* from DFT to GW+BSE calculations[14,34]. In the present work, we used the second approach to obtain DFT spinorial wave functions and feed them as input to GW and BSE calculations. It can be expected that there should be some difference between the effects of SOC, included by the two different approaches, on the energetic ordering of the $X_2$ and $X_3$ excitons and thus on their crossing and possible mixing induced by strain. However, the second approach to including SOC is in general more consistent and accurate.

Fig. 2(d) shows that the binding energies ($E_b$) of the $X_1$, $X_2$ and $X_3$ excitons, obtained from the difference between the excitonic and quasi-particle excitation energies, decrease monotonically and almost linearly with increasing $\epsilon$ from 0 to 5%. The intralayer excitons $X_2$ and $X_3$ are found to be more sensitive to the applied strain than the interlayer exciton $X_1$. Because $E_b$ decreases almost linearly with $\epsilon$ for the $X_1$, $X_2$ and $X_3$ excitons, we used the linear fitting to derive the sensitivities of these three excitons to the applied strain, indicated by $S_{X_1}$, $S_{X_2}$, and $S_{X_3}$. The fitted sensitivities of the $X_1$, $X_2$ and $X_3$ excitons are $S_{X_1} = -4.2$ meV/%, $S_{X_2} = -7.9$meV/%, and $S_{X_3} = -7.4$ meV/%, respectively. Moreover, the binding energy of the interlayer exciton $X_1$ is comparable to the binding energies of the intralayer excitons $X_2$ and $X_3$, e.g., $E_b = 255$ meV for $X_1$, 325 meV for $X_2$, and 295 meV for $X_3$, at $\epsilon = 0$. This appears counter-intuitive because interlayer excitons are formed by spatially separated electrons and holes. However, the spatial separation of the electron-hole interaction in a vertical heterobilayer could be compensated by the reduced Coulomb screening in the perpendicular direction of the vertical heterobilayer. Our results of the binding energies of interlayer and intralayer excitons in the absence of strain are in agreement with previous theoretical work[34,35]. Our results also show that under in-plane biaxial strain, interlayer excitons are less affected than intralayer excitons. The reason for this behavior is that in-plane biaxial strain tends to increase the electron-hole separation for both intralayer and interlayer excitons, leading to a decrease in their binding energies. However, interlayer excitons are also affected by a counteractive effect: Such strain at the same time tends to decrease in electron-hole separation for interlayer excitons, leading to an increase in their binding energy. This counteractive effect is absent for intralayer excitons, which makes them more sensitive to in-plane biaxial strain. This implies that excitons in monolayers are expected to be more efficiently tuned by in-plane biaxial strain due to the absence of interlayer coupling.

Previous experimental and theoretical studies of TMD monolayers and bilayers have shown the redshifts of exciton binding and excitation energies induced by in-plane biaxial strain are of the order of several to a few tens of meV per 1% strain[60,61]. For instance, theoretical calculations have found

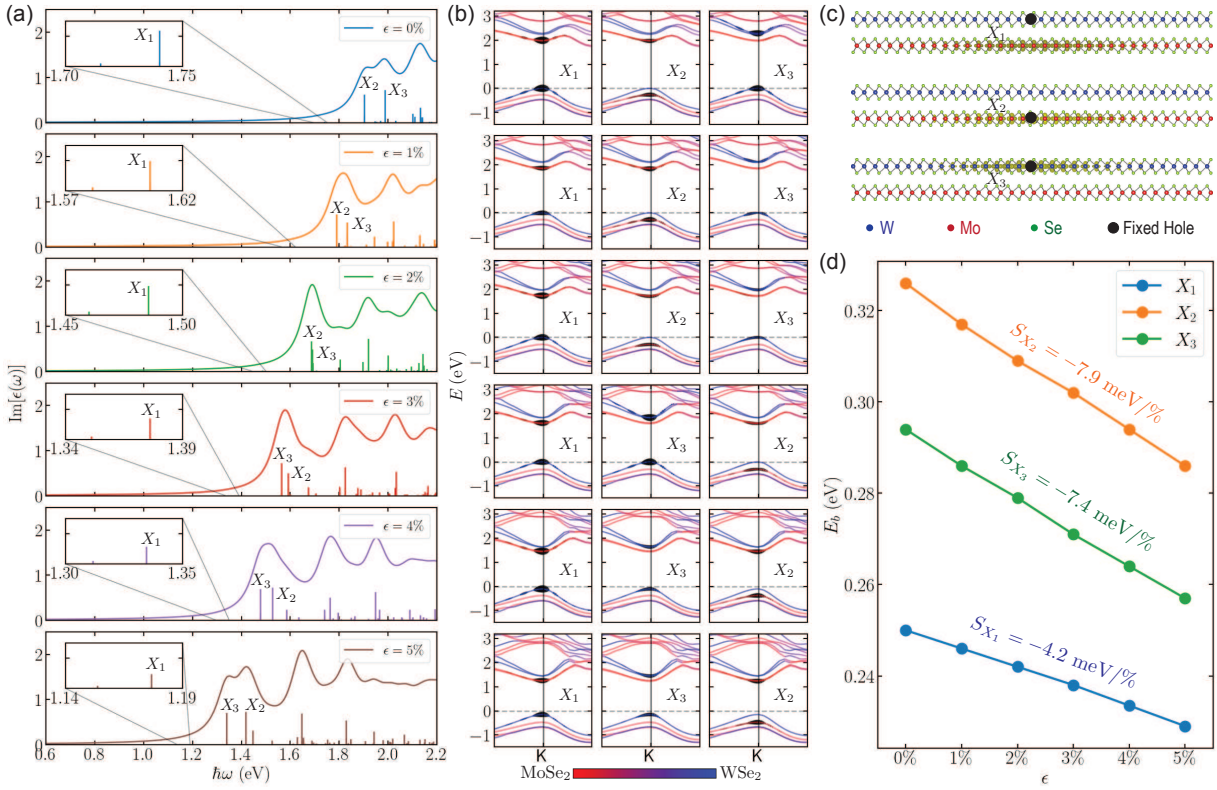


Figure 2. The strain dependence of the exciton states in vertically $AA'$-stacked $MoSe_2/WSe_2$ heterobilayer: (a) absorption spectra and oscillator strengths, (b) electron-hole weights on quasi-particle band structures, (c) spatial wave functions, and (d) binding energies. Here, $X_1$, $X_2$, and $X_3$ in (a-d) represent the three dominant exciton states in the on-set of absorption in (a), the black dots on the quasi-particle band structures in (b) indicate the electron-hole weights of the $X_1$, $X_2$, and $X_3$ excitons, the wave functions with the fixed hole positions in (c) characterize the spatial characters of the $X_1$, $X_2$, and $X_3$ excitons in the absence of strain, and $S_{X_1}$, $S_{X_2}$, and $S_{X_3}$ in (d) represent the sensitivities of the binding energies of the $X_1$, $X_2$, and $X_3$ excitons to the applied strain.

that the redshifts of exciton binding energy are 8 meV/% for WSe2 monolayer and 11 meV/% for MoS2 monolayer[60]. In our work, the redshifts of exciton binding energy were found to be 7.8 meV/% and 7.4 meV/% for intra-MoSe2-layer and intra-WSe2-layer excitons, respectively. The difference between those redshifts and our results is mainly caused by different reduced effective masses and dielectric constants (both of which can be changed by strain) due to the absence or presence of interlayer coupling.

It should be noted that in our GW and BSE calculations, substrate dielectric screening was not taken into account, which plays an important role on quasi-particle and excitonic properties. Coulomb interaction can be reduced by such screening, which leads to the reduction of both quasi-particle band gap (calculated with GW) and exciton binding energy (calculated with BSE). However, because both reduction tend to be canceled out, excitonic absorption spectrum is expected to be less affected by substrate dielectric screening. Theoretically, substrate dielectric screening in 2D materials can be included in both first-principles and effective-model calculations. In first-principles calculations, substrate dielectric screening can be modeled as a substrate material supporting a 2D material, where lattice mismatch between them needs to be minimized using the supercell approach. Such a system is often composed of many atoms due to (1) the large thickness of substrate material and (2) the lattice mismatch leading to a possibly large supercell. This would make first-principles calculations of substrate dielectric screening prohibitively demanding, especially for those including many-body effects such as quasi-particle and excitonic effects. However, this limitation can be overcome by effective-model calculations, which use minimal parameters such as effective mass and dielectric constant. For instance, the effect of substrate dielectric screening on the exciton binding energy in a 2D system can be calculated using an effective-mass model Hamiltonian with a non-locally screened Coulomb potential in the 2D limit[70].

Finally, we should mention that in our BSE calculations only *momentum-direct* excitons were included, while the possible contribution of *momentum-indirect* excitons was neglected. Momentum-indirect excitons of interlayer character have been proposed to be the origin of the prominent peak at the excitation energy of 1.6 eV in the PL spectrum observed for vertical $MoS_2/WSe_2$ heterostructures[39]. It can be expected that compared to momentum-direct excitons, momentum-indirect excitons would have a much weaker layer confinement and thus a more extended spatial separation of coupled electrons and holes if $\Gamma$ or Q points are involved

in the formation of these excitons because of interlayer hybridization at these points in the Brillouin zone[41]. The layer-projected band structure can be used to analyze the interlayer hybridization degrees of the electron and hole states at K, Q, and Γ points. Due to interlayer hybridization, momentum indirect and direct excitons have typically different dipole oscillator strengths. Depending on the orbital character of the valence and conduction bands, momentum-indirect excitons have either smaller or larger dipole oscillator strength than their momentum-direct counterparts[40]. For instance, for those formed by K-point electrons and Γ-point holes (i.e. Γ-K excitons), their oscillator strength should be typically smaller than K-K excitons that are formed by electrons and holes both residing at K point[41]. As for the strain-dependence, we expect the momentum-indirect excitons involving Γ and Q points to qualitatively lie in between the intralayer excitons and the K-K interlayer excitons, due to the increased spatial overlap electron and hole contributions to the exciton wave functions as a results of stronger interlayer hybridization. Therefore, it would be interesting to study the effect of strain on momentum-indirect interlayer and intralayer excitons in the near future.

To conclude, we investigated the quasi-particle and excitonic properties of vertically $AA'$-stacked $MoSe_2$/$WSe_2$ heterobilayer in the presence of in-plane biaxial strain of up to 5% using density-function theory calculations with many-body effects. We calculated the strain dependence of quasi-particle band structure, exciton absorption spectrum, oscillator strength, wave function, and binding energy by solving the BSE on top of the GW approach. We showed that the quasi-particle band structure exhibits the type-II alignment leading to spatially separated electrons and holes localized in the $MoSe_2$ and $WSe_2$, respectively. The quasi-particle band gap is found to be globally indirect in the absence of strain whereas it can be direct or indirect in the presence of strain, depending on the magnitude the strain. We identified the interlayer and intralayer excitons by analysing their electron-hole weights in reciprocal space and wave functions in real space. We showed that with increasing strain magnitude, the absorption spectrum of the interlayer and intralayer excitons is red-shifted and re-ordered, and the binding energies of these layer-resolved excitons decrease monotonically and almost linearly. We derived the sensitivity of exciton binding energy to the applied strain and found that the intralayer excitons are more sensitive to strain than interlayer excitons. For instance, the derived sensitivities are $-4.2$ meV/% for the interlayer excitons, $-7.9$ meV/% for the intra-$MoS_2$-layer excitons, and $-7.4$ meV/% for the intra-$WS_2$-layer excitons. Moreover, we found that the interlayer and intralayer excitons have comparable binding energies of the order of 250 (300) meV for the former (latter) in the absence of strain. Our results indicated interlayer and intralayer excitons in vertically $AA'$-stacked $MoSe_2$/$WSe_2$ heterobilayer are highly tunable by in-plane biaxial strain.

This work was supported by the Flemish Science Foundation (FWO-Vl). Computational resources were provided by the Flemish Supercomputer Center (VSC).

* longlong.li@uantwerpen.be
† roland.gillen@fau.de
‡ maurizia.palummo@roma2.infn.it
§ milorad.milosevic@uantwerpen.be
¶ francois.peeters@uantwerpen.be

[1] B. Radisavljevic, A. Radenovic, J. Brivio, V. Giacometti, and A. Kis, Nat. Nanotech **6**, 147 (2011).
[2] O. Lopez-Sanchez, D. Lembke, M. Kayci, A. Radenovic, and A. Kis, Nat. Nanotech. **8**, 497 (2013).
[3] Q. H. Wang, K. Kalantar-Zadeh, A. Kis, J. N. Coleman, and M. S. Strano, Nat. Nanotech. **7**, 699 (2012).
[4] K. F. Mak and J. Shan, Nat. Photon. **10**, 216 (2016).
[5] K. He, N. Kumar, L. Zhao, Z. Wang, K. F. Mak, H. Zhao, and J. Shan, Phys. Rev. Lett. **113**, 026803 (2014).
[6] H. M. Hill, A. F. Rigosi, C. Roquelet, A. Chernikov, T. C. Berkelbach, D. R. Reichman, M. S. Hybertsen, L. E. Brus, and T. F. Heinz, Nano Lett. **15**, 2992 (2015).
[7] A. R. Klots, A. K. M. Newaz, B. Wang, D. Prasai, H. Krzyzanowska, J. Lin, D. Caudel, N. J. Ghimire, J. Yan, B. L. Ivanov, K. A. Velizhanin, A. Burger, D. G. Mandrus, N. H. Tolk, S. T. Pantelides, and K. I. Bolotin, Sci. Rep. **4**, 6608 (2014).
[8] A. F. Rigosi, H. M. Hill, K. T. Rim, G. W. Flynn, and T. F. Heinz, Phys. Rev. B **94**, 075440 (2016).
[9] M. M. Ugeda, A. J. Bradley, S.-F. Shi, F. H. da Jornada, Y. Zhang, D. Y. Qiu, W. Ruan, S.-K. Mo, Z. Hussain, Z.-X. Shen, F. Wang, S. G. Louie, and M. F. Crommie, Nat. Mater. **13**, 1091 (2014).
[10] B. Zhu, X. Chen, and X. Cui, Sci. Rep. **5**, 9218 (2015).
[11] G. Wang, A. Chernikov, M. M. Glazov, T. F. Heinz, X. Marie, T. Amand, and B. Urbaszek, Rev. Mod. Phys. **90**, 021001 (2018).
[12] K. F. Mak, C. Lee, J. Hone, J. Shan, and T. F. Heinz, Phys. Rev. Lett. **105**, 136805 (2010).
[13] A. Ramasubramaniam, Phys. Rev. B **86**, 115409 (2012).
[14] A. Molina-Sánchez, D. Sangalli, K. Hummer, A. Marini, and L. Wirtz, Phys. Rev. B **88**, 045412 (2013).
[15] D. Y. Qiu, F. H. da Jornada, and S. G. Louie, Phys. Rev. Lett. **111**, 216805 (2013).
[16] K. M. McCreary, A. T. Hanbicki, S. V. Sivaram, and B. T. Jonker, APL Mater. **6**, 111106 (2018).
[17] A. Carvalho, R. M. Ribeiro, and A. H. Castro Neto, Phys. Rev. B **88**, 115205 (2013).
[18] R. Gillen and J. Maultzsch, IEEE J. Sel. Top. Quantum Electron. **23**, 219 (2017).
[19] R. Gillen, Phys. Status Solidi B **258**, 2170031 (2021).
[20] T. C. Berkelbach, M. S. Hybertsen, and D. R. Reichman, Phys. Rev. B **88**, 045318 (2013).
[21] K. F. Mak, K. He, C. Lee, G. H. Lee, J. Hone, T. F. Heinz, and J. Shan, Nat. Mater. **12**, 207 (2013).
[22] J. S. Ross, S. Wu, H. Yu, N. J. Ghimire, A. M. Jones, G. Aivazian, J. Yan, D. G. Mandrus, D. Xiao, W. Yao, and X. Xu, Nat. Commun. **4**, 1474 (2013).
[23] Y. You, X.-X. Zhang, T. C. Berkelbach, M. S. Hybertsen, D. R. Reichman, and T. F. Heinz, Nat. Phys. **11**, 477 (2015).
[24] M. Van der Donck, M. Zarenia, and F. M. Peeters, Phys. Rev. B **97**, 195408 (2018).
[25] A. Steinhoff, M. Florian, A. Singh, K. Tran, M. Kolarczik, S. Helmrich, A. W. Achtstein, U. Woggon, N. Owschimikow,

F. Jahnke, and X. Li, Nature Phys **14**, 1199 (2018).
[26] R. Cheng, D. Li, H. Zhou, C. Wang, A. Yin, S. Jiang, Y. Liu, Y. Chen, Y. Huang, and X. Duan, Nano Lett. **14**, 5590 (2014).
[27] P. Rivera, J. R. Schaibley, A. M. Jones, J. S. Ross, S. Wu, G. Aivazian, P. Klement, K. Seyler, G. Clark, N. J. Ghimire, J. Yan, D. G. Mandrus, W. Yao, and X. Xu, Nat. Commun. **6**, 6242 (2015).
[28] Y. Yu, S. Hu, L. Su, L. Huang, Y. Liu, Z. Jin, A. A. Purezky, D. B. Geohegan, K. W. Kim, Y. Zhang, and L. Cao, Nano Lett. **15**, 486 (2015).
[29] D. Kozawa, A. Carvalho, I. Verzhbitskiy, F. Giustiniano, Y. Miyauchi, S. Mouri, A. H. Castro Neto, K. Matsuda, and G. Eda, Nano Lett. **16**, 4087 (2016).
[30] B. Miller, A. Steinhoff, B. Pano, J. Klein, F. Jahnke, A. Holleitner, and U. Wurstbauer, Nano Lett. **17**, 5229 (2017).
[31] J. S. Ross, P. Rivera, J. Schaibley, E. Lee-Wong, H. Yu, T. Taniguchi, K. Watanabe, J. Yan, D. Mandrus, D. Cobden, W. Yao, and X. Xu, Nano Lett. **17**, 638 (2017).
[32] J. Kang, S. Tongay, J. Zhou, J. Li, and J. Wu, Appl. Phys. Lett. **102**, 012111 (2013).
[33] M. Palummo, M. Bernardi, and J. C. Grossman, Nano Lett. **15**, 2794 (2015).
[34] R. Gillen and J. Maultzsch, Phys. Rev. B **97**, 165306 (2018).
[35] E. Torun, H. P. C. Miranda, A. Molina-Sánchez, and L. Wirtz, Phys. Rev. B **97**, 245427 (2018).
[36] T. Deilmann and K. S. Thygesen, Nano Lett. **18**, 2984 (2018).
[37] B. Miller, A. Steinhoff, B. Pano, J. Klein, F. Jahnke, A. Holleitner, and U. Wurstbauer, Nano Lett. **17**, 5229 (2017).
[38] A. T. Hanbicki, H.-J. Chuang, M. R. Rosenberger, C. S. Hellberg, S. V. Sivaram, K. M. McCreary, I. I. Mazin, and B. T. Jonker, ACS Nano **12**, 4719 (2018).
[39] J. Kunstmann, F. Mooshammer, P. Nagler, A. Chaves, F. Stein, N. Paradiso, G. Plechinger, C. Strunk, C. Schüller, G. Seifert, D. R. Reichman, and T. Korn, Nat. Phys. **14**, 801 (2018).
[40] T. Deilmann and K. S. Thygesen, 2D Mater. **6**, 035003 (2019).
[41] R. Gillen, Phys. Status Solidi B **258**, 2000614 (2021).
[42] F. Wu, T. Lovorn, and A. H. MacDonald, Phys. Rev. Lett. **118**, 147401 (2017).
[43] N. Zhang, A. Surrente, M. Baranowski, D. K. Maude, P. Gant, A. Castellanos-Gomez, and P. Plochocka, Nano Lett. **18**, 7651 (2018).
[44] K. Tran, G. Moody, F. Wu, X. Lu, J. Choi, K. Kim, A. Rai, D. A. Sanchez, J. Quan, A. Singh, J. Embley, A. Zepeda, M. Campbell, T. Autry, T. Taniguchi, K. Watanabe, N. Lu, S. K. Banerjee, K. L. Silverman, S. Kim, E. Tutuc, L. Yang, A. H. MacDonald, and X. Li, Nature **567**, 71 (2019).
[45] C. Jin, E. C. Regan, A. Yan, M. Iqbal Bakti Utama, D. Wang, S. Zhao, Y. Qin, S. Yang, Z. Zheng, S. Shi, K. Watanabe, T. Taniguchi, S. Tongay, A. Zettl, and F. Wang, Nature **567**, 76 (2019).
[46] L. Zhang, Z. Zhang, F. Wu, D. Wang, R. Gogna, S. Hou, K. Watanabe, T. Taniguchi, K. Kulkarni, T. Kuo, S. R. Forrest, and H. Deng, Nat. Commun. **11**, 5888 (2020).
[47] D. A. Ruiz-Tijerina, I. Soltero, and F. Mireles, Phys. Rev. B **102**, 195403 (2020).
[48] S. Brem, C. Linderälv, P. Erhart, and E. Malic, Nano Lett. **20**, 8534 (2020).
[49] J. Choi, M. Florian, A. Steinhoff, D. Erben, K. Tran, D. S. Kim, L. Sun, J. Quan, R. Claassen, S. Majumder, J. A. Hollingsworth, T. Taniguchi, K. Watanabe, K. Ueno, A. Singh, G. Moody, F. Jahnke, and X. Li, Phys. Rev. Lett. **126**, 047401 (2021).
[50] M. Förg, A. S. Baimuratov, S. Y. Kruchinin, I. A. Vovk, J. Scherzer, J. Förste, V. Funk, K. Watanabe, T. Taniguchi, and A. Högele, Nat. Commun. **12**, 1656 (2021).
[51] W. Zheng, L. Xiang, F. A. de Quesada, M. Augustin, Z. Lu, M. Wilson, A. Sood, F. Wu, D. Shcherbakov, S. Memaran, R. E. Baumbach, G. T. McCandless, J. Y. Chan, S. Liu, J. H. Edgar, C. N. Lau, C. H. Lui, E. J. G. Santos, A. Lindenberg, D. Smirnov, and L. Balicas, ACS Nano **16**, 18695 (2022).
[52] E. Barré, O. Karni, E. Liu, A. L. O'Beirne, X. Chen, H. B. Ribeiro, L. Yu, B. Kim, K. Watanabe, T. Taniguchi, K. Barmak, C. H. Lui, S. Refaely-Abramson, F. H. da Jornada, and T. F. Heinz, Science **376**, 406 (2022).
[53] R. Roldán, A. Castellanos-Gomez, E. Cappelluti, and F. Guinea, J. Phys.: Condens. Matter **27**, 313201 (2015).
[54] H. J. Conley, B. Wang, J. I. Ziegler, R. F. Haglund, S. T. Pantelides, and K. I. Bolotin, Nano Lett. **13**, 3626 (2013).
[55] K. He, C. Poole, K. F. Mak, and J. Shan, Nano Lett. **13**, 2931 (2013).
[56] Y. Y. Hui, X. Liu, W. Jie, N. Y. Chan, J. Hao, Y.-T. Hsu, L.-J. Li, W. Guo, and S. P. Lau, ACS Nano **7**, 7126 (2013).
[57] H. Shi, H. Pan, Y.-W. Zhang, and B. I. Yakobson, Phys. Rev. B **87**, 155304 (2013).
[58] R. Schmidt, I. Niehues, R. Schneider, M. Drüppel, T. Deilmann, M. Rohlfing, S. M. de Vasconcellos, A. Castellanos-Gomez, and R. Bratschitsch, 2D Mater. **3**, 021011 (2016).
[59] R. K. Defo, S. Fang, S. N. Shirodkar, G. A. Tritsaris, A. Dimoulas, and E. Kaxiras, Phys. Rev. B **94**, 155310 (2016).
[60] M. Feierabend, A. Morlet, G. Berghäuser, and E. Malic, Phys. Rev. B **96**, 045425 (2017).
[61] F. Carrascoso, D.-Y. Lin, R. Frisenda, and A. Castellanos-Gomez, J. Phys. Mater. **3**, 015003 (2020).
[62] F. Carrascoso, H. Li, R. Frisenda, and A. Castellanos-Gomez, Nano Res. **14**, 1698 (2021).
[63] C. Cho, J. Wong, A. Taqieddin, S. Biswas, N. R. Aluru, S. Nam, and H. A. Atwater, Nano Lett. **21**, 3956 (2021).
[64] B. Aslan, M. Deng, and T. F. Heinz, Phys. Rev. B **98**, 115308 (2018).
[65] Z. Khatibi, M. Feierabend, M. Selig, S. Brem, C. Linderälv, P. Erhart, and E. Malic, 2D Mater. **6**, 015015 (2018).
[66] K. Zollner, P. E. F. Junior, and J. Fabian, Phys. Rev. B **100**, 195126 (2019).
[67] R. Rosati, S. Brem, R. Perea-Causín, R. Schmidt, I. Niehues, S. M. d. Vasconcellos, R. Bratschitsch, and E. Malic, 2D Mater. **8**, 015030 (2020).
[68] B. Aslan, C. Yule, Y. Yu, Y. J. Lee, T. F. Heinz, L. Cao, and M. L. Brongersma, 2D Mater. **9**, 015002 (2021).
[69] T. Cheiwchanchamnangij and W. R. L. Lambrecht, Phys. Rev. B **85**, 205302 (2012).
[70] T. C. Berkelbach, M. S. Hybertsen, and D. R. Reichman, Phys. Rev. B **88**, 045318 (2013).

# Supplemental Material for "Strain tunable interlayer and intralayer excitons in vertically stacked $MoSe_2/WSe_2$ heterobilayers"

L. L. Li,[1,2] R. Gillen,[3] M. Palummo,[4] M. V. Milošević,[2] and F. M. Peeters[2]

[1]*School of Physics and Optoelectronic Engineering, Nanjing University of Information Science and Technology, Nanjing 210044, China*

[2]*Department of Physics, University of Antwerp, Groenenborgerlaan 171, 2020 Antwerpen, Belgium*

[3]*Friedrich-Alexander Universität Erlangen-Nürnberg, Staudtstrasse 7, 91058 Erlangen, Germany*

[4]*Dipartimento di Fisica and INFN, Universit?di Roma Tor Vergata, Via della Ricerca Scientifica 1, 00133 Rome, Italy*

(Dated: August 31, 2023)

In this supplemental material, we present (1) the theoretical approach used in the manuscript and (2) the supplementary results including Table. S1, Fig. S1, Fig. S2, Fig. S3, Fig. S4, Fig. S5, and Fig. S6.

PACS numbers:

## I. THEORETICAL APPROACH

The atomic positions and the cell parameters of vertically stacked $MoSe_2/WSe_2$ heterobilayers in the presence of in-plane biaxial strain were relaxed using the VASP code [1] in the Perdew-Burke-Ernzerhof (PBE) approximation [2] with the DFT-D3 vdW correction [3]. An energy cutoff of 500 eV was used in the plane-wave expansion and a Γ-centered **k**-grid of $12 \times 12 \times 1$ was used to sample the Brillouin zone. The vacuum thickness between two periodic images was set to 20 Å. The in-plane biaxial strain was modeled and defined as $\epsilon = (a - a_0)/a_0$ with $a$ ($a_0$) the in-plane lattice constant of strained (unstrained) heterobilayers. The structural relaxation was converged when the forces on atoms were less than $10^{-3}$ eV/Å and the change of electronic total energy was less than $10^{-6}$ eV.

The electronic ground states of the relaxed heterobilayers were obtained using the QUANTUM ESPRESSO code [4] in the PBE approximation [2] using fully relativistic norm-conserving pseudopotentials [5] with inclusion of the semicore $s$ and $p$ orbitals of Mo and W. The plane-wave energy cutoff in the ground-state calculations was set to 60 Ry. The self-consistency was achieved when the change of electronic total energy was less than $10^{-8}$ Ry.

The excitonic states and their absorption spectra of the relaxed heterobilayers were calculated by solving the Bethe-Salpeter equation (BSE) [6] using the YAMBO code [7, 8]. The single-particle energies obtained from DFT were corrected by the standard $G_0W_0$ approach [9] in the plasmon-pole approximation [10]. The BSE calculations were performed on top of the quasi-particle energies on a Γ-centered **k**-grid of $33 \times 33 \times 1$. A full spin-orbit interaction was included to account for the spin-orbit splitting of the valence and conduction bands. An exchange cutoff of 60 Ry, a response cutoff of 10 Ry, and 400 single-particle bands were used to calculate the self-energies and the response functions. The 10 highest valence bands and the 10 lowest conduction bands were used to calculate the excitonic states, on top of which a Lorentzian broadening of 0.05 eV was used to calculate the absorption spectra. Our systematic convergence study indicates that the quasi-particle band gap and the excitonic absorption spectrum were reasonably converged with the aforementioned parameters, i.e., the number of bands, the number of **k**-points, and the response cutoff (see Fig. S1 and Fig. S2).

In both the $G_0W_0$ and BSE calculations, the effective energy technique [11] was used to

include the contribution from high-energy unoccupied bands. The Coulomb truncation technique [12] was used to eliminate spurious interaction between periodic images of confined systems. The Coulomb truncation is crucially important for 2D materials and their heterostructures because of their strong confinement in the out-of-plane direction. The Monte Carlo integration was used to average the head of the screened Coulomb interaction by using a model dielectric function in the vicinity of the Γ point [13].

## II. SUPPLEMENTARY RESULTS

Table. S1 shows the relaxed lattice parameters and the total electron energies for different stacking orders of vertical $MoSe_2/WS_2$ heterobilayer in the absence of strain. We compared the relaxed lattice constant and interlayer distance that were obtained in the present work using the VASP code against those that were obtained in the previous work using the Quantum Espresso code [13]. Here, both the calculations were performed using the converged parameters in the PBE approximation with the DFT-D3 vdW coorection. As can be seen, for all three different stackings (AA, AB, and AA'), the values of lattice constant and interlayer distance obtained using VASP are very close to those obtained using QE. For instance, the maximum relative error for the lattice constant is less than 0.1%. Moreover, both codes derived the same conclusion that AA' stacking is energetically the most stable configuration. We also want to stress that the overlap between the VASP and the QE calculations is the lattice vectors relaxed by VASP for the strain-free (and correspondingly also the strained) MoSe2/WSe2 heterobilayers. The lattice vectors were then kept fixed and the atomic positions were re-optimized by QE, before the electronic structures and optical properties were calculated. Due to the very small difference in lattice constants between VASP and QE for the strain-free system, we expect minor effects on our results obtained from this procedure, e.g., the slopes of the strain-dependent band gap and exciton binding energy shifts should not be affected.

Figs. S1 shows the convergence study of the quasi-particle band gap with respect to the number of empty bands and the cutoff of dielectric function, and Figs. S2 the convergence study of the quasi-particle band gap and excitonic absorption spectrum with respect to the number of **k**-points. Based on these convergence studies, we took the exchange cutoff of 60 Ry, the response cutoff of 10 Ry, and 400 single-particle bands, the **k**-point of $33 \times 33 \times 1$.

Fig. S3 shows (a) the interlayer exciton wave functions with fixed hole position at 0% and 2% strain and (b) the corresponding Gaussian fits as a function of the position along the bisecting line of the supercell (see the black line in the inset). In order to quantify the difference, we attempted to estimate the spatial extents of the exciton wave functions by first projecting them onto the 2D plane $x$-$y$ plane, then taking a diagonal line that bisects the supercell and crosses its central point [see the black line in the inset of (b)], and finally fitting Gauss functions to the projected results along this diagonal line. As can be seen, while the interlayer exciton wave functions obtained with and without strain appear to be quite similar, the fitted Gaussians suggest a slightly larger spatial extent in the strained case. This is further highlighted in the difference between the fitted Gaussians. The FWHM of the Gaussians differ by about 2%, suggesting mainly a geometrical effect due to expansion of the Mo-Mo and W-W distances. So the effect of strain is mainly expanding the exciton wave functions together with the atomic positions.

Fig. S4 shows the vertical positions of the Mo, W, and Se atoms as well as the interlayer distance as a function of strain. As can be seen, with increasing strain magnitude, the vertical positions of Mo and W (in $z$ direction) increases (decreases) from 11.68 (18.20) Å to 11.74 (18.13) Å , leading to reduction of the interlayer distance $d$ from 6.52 Å to 6.39 Å . The Se atoms on the outer layers (Se1 and Se4) show the similar variation with strain as the Mo and W atoms, whereas the Se atoms on the inner layers (Se2 and Se3) remain almost unchanged with strain. We also attached in the Appendix of the Supplemental Material the relaxed structures of the strained $MoSe_2/WSe_2$ heterobilayers in the format of VASP POSCAR.

Fig. S5 shows the comparison between the DFT-D2 and DFT-D3 results: (a) and (b) The DFT-D2 and DFT-D3 band structures, respectively, in the absence of strain, and (c) the strain dependence of the DFT-D2 and DFT-D3 direct band gaps. As can be seen in (a) and (b), in the absence of strain, the DFT-D3 band structure exhibits a globally indirect band gap whereas the DFT-D2 band structure displays a globally direct band gap. However, as shown in (c), the strain dependence of the DFT-D3 direct band gap is very similar to that of the DFT-D2 direct band gap (the latter can be viewed almost the same as the former by shifting the latter upwards about 80 meV). This is not surprising, as the vdW corrections only add contributions to the total energy, the interatomic forces and the cell stress, while the electrnic band structure is calculated from DFT-PBE, with only indrect effects from the vDw

correction through the changed geometry. Therefore, in terms of momentum-direct excitons considered in our work, it can be expected that the DFT-D2 and DFT-D3 vdW corrections should give qualitatively similar results. Moreover, it has been shown [14] that for various standard energy benchmark sets, DFT-D4 only slightly outperforms DFT-D3 especially for metal containing systems. As DFT-D3 already rather accurately reproduces experimental interlayer distances and intralayer lattice constants, we expect only minor differences in the geometry, and thus the deduced strain behavior of the electronic bandstructure, compared to simulations using DFT-D4 vdW corrections.

Fig. S6 shows the $G_0W_0$ band structure at zero strain [(a)] and the $G_0W_0$ energies of the lowest conduction band (LCB) and the highest valence band (HVB) at K, Q, and Γ as a function of strain [(b) and (c)]. The globally direct or indirect nature of the $G_0W_0$ band gap can be understood with the location of the valence-band maximum (VBM) and the conduction-band minimum (CBM) in the quasi-particle band structure. As can been seen, the $G_0W_0$ VBM and CBM are located at K and Q, respectively, for zero and 1% strain, while the $G_0W_0$ CBM is shifted from Q to K for 2% and 3% strain, leading to a direct band gap. For 4% and 5% strain, the $G_0W_0$ VBM is shifted as well, from K to Γ, restoring to an indirect band gap. If the convergence is further increased (e.g. the number of bands and the number of kpoints), the general feature of the $G_0W_0$ band gap should remain the same, i.e., it undergoes globally from indirect to direct and back to indirect. However, the critical strain values at those transitions are expected to be different than 2% and 3%.

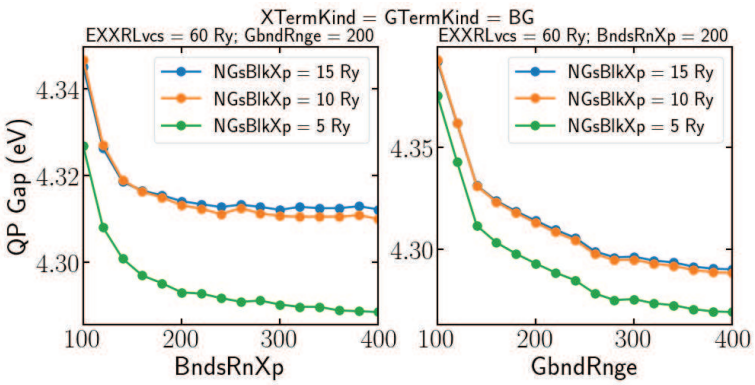


FIG. S1: (Convergence study of the $G_0W_0$ band gap at the $\Gamma$ point with respect to the number of empty bands (BndsRnXp and GbndRnge) and the cutoff of dielectric function (NGsBlkXp). Here, a **k**-grid of $12 \times 12 \times 1$ was used in the $G_0W_0$ calculation.

TABLE S1: The in-plane lattice constant ($a$), the interlayer distance between the top and bottom metal planes ($d$), and the total electron energy ($E_{tot}$) in $AA$-, $AA'$-, and $AB$-stacked $MoSe_2/WS_2$ heterobilayers. The results obtained in the present work were calculated using the VASP code, which are compared to those that were obtained in the previous work [13] using the Quantum Espresso (QE) code.

| | VASP* | | | QE** | |
|---|---|---|---|---|---|
| Stacking | $a$ (Å) | $d$ (Å) | $E_{tot}$ (eV) | $a$ (Å) | $d$ (Å) |
| $AA$ | 3.291 | 7.101 | −42.999 | 3.290 | 7.097 |
| $AA'$ | 3.290 | 6.523 | −43.084 | 3.293 | 6.512 |
| $AB$ | 3.292 | 6.529 | −43.079 | 3.293 | 6.474 |

*The present work.
**The previous work [13].

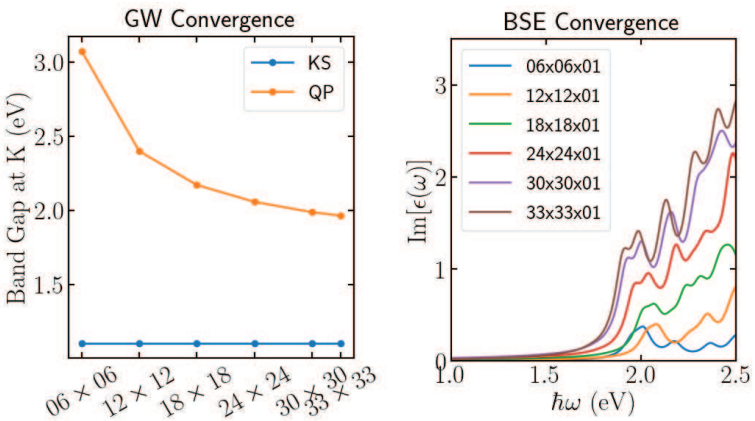


FIG. S2: (Convergence study of the $G_0W_0$ band gap (at the K point) and the BSE absorption spectrum with respect to the number of **k**-points. Here, the parameters BndsRnXp=GbndRnge=200 and NGsBlkXp=10 were used in the $G_0W_0$ and BSE calculations.

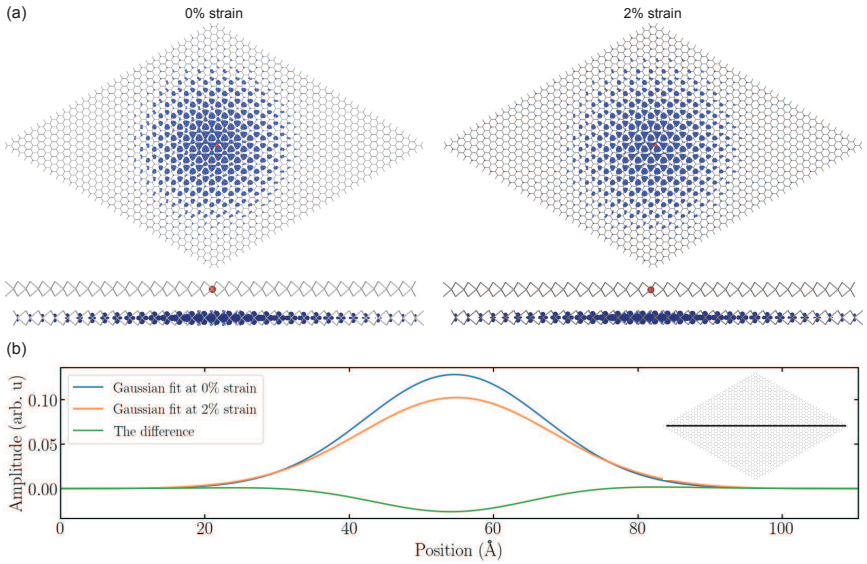


FIG. S3: (a) Top and side views of the interlayer exciton wave functions with fixed hole position at 0% and 2% strain, and (b) their Gaussian fits as a function of the position along the bisecting line of the supercell (see the black line in the inset). The red dots in (a) indicate the fixed hole positions (located on the W atom) in the absence and presence of strain.

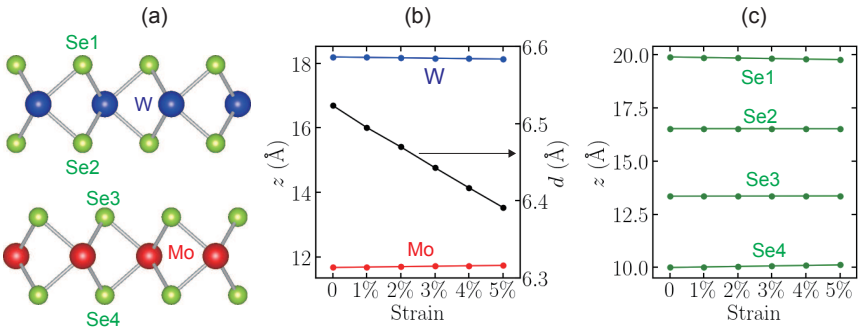


FIG. S4: (a) Side view of the lattice structure of $MoSe_2WSe_2$ heterobilayer, (b) the vertical positions of Mo and W and the interlayer distance as a function of strain, and (c) the vertical positions of Se in the outer (Se1 and Se4) and inner (Se2 and Se3) atomic layers.

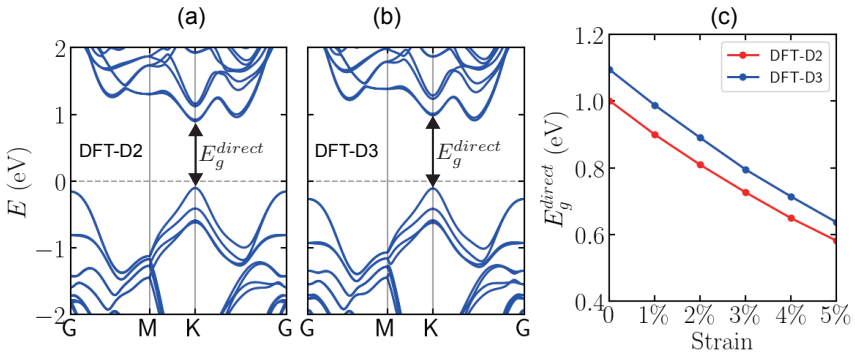


FIG. S5: (a) and (b) The DFT-D2 and DFT-D3 band structures at zero strain, and (c) the DFT-D2 and DFT-D3 direct band gap as a function of strain.

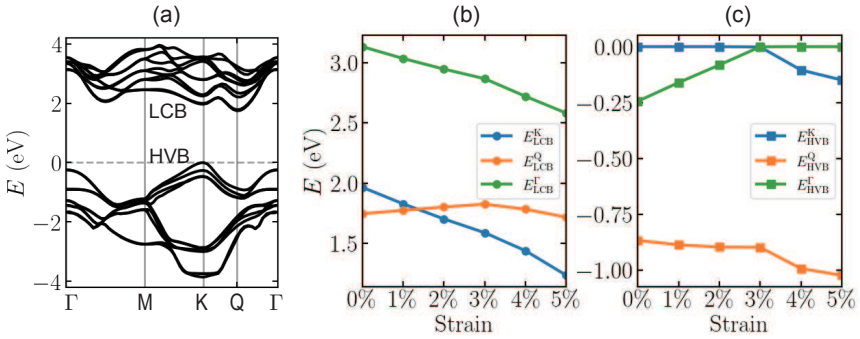


FIG. S6: (a) The quasi-particle band structure at zero strain, (b) the quasi-particle energies of the lowest conduction band (LCB) at K, Q, and Γ points, and (c) the quasi-particle energies of the highest valence band (HVB) at K, Q, and Γ points.

[1] G. Kresse and J. Furthmüller, Phys. Rev. B **54**, 11169 (1996).

[2] J. P. Perdew, K. Burke, and M. Ernzerhof, Phys. Rev. Lett. **77**, 3865 (1996).

[3] S. Grimme, J. Antony, S. Ehrlich, and H. Krieg, J. Chem. Phys. **132**, 154104 (2010).

[4] P. Giannozzi, S. Baroni, N. Bonini, M. Calandra, R. Car, C. Cavazzoni, D. Ceresoli, G. L. Chiarotti, M. Cococcioni, I. Dabo, A. D. Corso, S. de Gironcoli, S. Fabris, G. Fratesi, R. Gebauer, U. Gerstmann, C. Gougoussis, A. Kokalj, M. Lazzeri, L. Martin-Samos, N. Marzari, F. Mauri, R. Mazzarello, S. Paolini, A. Pasquarello, L. Paulatto, C. Sbraccia, S. Scandolo, G. Sclauzero, A. P. Seitsonen, A. Smogunov, P. Umari, and R. M. Wentzcovitch, J. Phys.: Condens. Matter **21**, 395502 (2009).

[5] M. Schlipf and F. Gygi, Comput. Phys. Commun. **196**, 36 (2015).

[6] M. Rohlfing and S. G. Louie, Phys. Rev. B **62**, 4927 (2000).

[7] A. Marini, C. Hogan, M. Grüning, and D. Varsano, Comput. Phys. Commun. **180**, 1392 (2009).

[8] D. Sangalli, A. Ferretti, H. Miranda, C. Attaccalite, I. Marri, E. Cannuccia, P. Melo, M. Marsili, F. Paleari, A. Marrazzo, G. Prandini, P. Bonfà, M. O. Atambo, F. Affinito, M. Palummo, A. Molina-Sánchez, C. Hogan, M. Grüning, D. Varsano, and A. Marini, J. Phys.: Condens. Matter **31**, 325902 (2019).

[9] G. Onida, L. Reining, and A. Rubio, Rev. Mod. Phys. **74**, 601 (2002).

[10] P. Larson, M. Dvorak, and Z. Wu, Phys. Rev. B **88**, 125205 (2013).

[11] F. Bruneval and X. Gonze, Phys. Rev. B **78**, 085125 (2008).

[12] S. Ismail-Beigi, Phys. Rev. B **73**, 233103 (2006).

[13] R. Gillen and J. Maultzsch, Phys. Rev. B **97**, 165306 (2018).

[14] E. Caldeweyher, S. Ehlert, A. Hansen, H. Neugebauer, S. Spicher, C. Bannwarth, and S. Grimme, J. Chem. Phys. **150**, 154122 (2019).